Thermomechanical Properties of Lignin-Based Electrospun Nanofibers and Films Reinforced with Cellulose Nanocrystals: A Dynamic Mechanical and Nanoindentation Study

Mariko Ago,*[,†,‡] Joseph E. Jakes,*[,§] and Orlando J. Rojas[†,‖]

[†]Departments of Forest Biomaterials and Chemical and Biomolecular Engineering, North Carolina State University, Raleigh, North Carolina 27695, United States

[‡]Faculty of Science and Engineering, Tokushima Bunri University, Sanuki, Kagawa 769-2101, Japan

[§]Forest Biopolymers Science and Engineering, United States Department of Agriculture Forest Service, Forest Products Laboratory, Madison, Wisconsin 53726, United States

[‖]Department of Forest Products Technology, School of Chemical Technology, Aalto University, FI-00076 Aalto, Espoo, Finland

S *Supporting Information*

ABSTRACT: We produced defect-free electrospun fibers from aqueous dispersions of lignin, poly(vinyl alcohol) (PVA), and cellulose nanocrystals (CNCs), which were used as reinforcing nanoparticles. The thermomechanical performance of the lignin-based electrospun fibers and the spin-coated thin films was improved when they were embedded with CNCs. Isochronal dynamic mechanical analysis (DMA) was used to assess the viscoelastic properties of the lignin:PVA electrospun fiber mats loaded with CNCs. DMA revealed that α relaxation processes became less prominent with an increased lignin content, an effect that correlated with the loss tangent ($\tan \delta = E''/E'$) and α peak (T_g) that shifted to higher temperatures. This can be ascribed to the restraint of the segmental motion of PVA in the amorphous regions caused by strong intermolecular interactions. The reinforcing effect and high humidity stability attained by addition of CNCs (5, 10, or 15 wt %) in the multicomponent fiber mats were revealed. Nanoindentation was performed to assess the elastic modulus and hardness of as-prepared and cross-section surfaces of spin-coated lignin:PVA (75:25) films loaded with CNC. The properties of the two surfaces differed, and only the trend in cross-section elastic modulus correlated with DMA results. After addition of 5 wt % CNCs, both the DMA and nanoindentation elastic modulus remained constant, while after addition of 15 wt % CNCs, both increased substantially. An indentation size effect was observed in the nanoindentation hardness, and the results provided insight into the effect of addition of CNCs on the microphysical processes controlling the yield behavior in the composites.

KEYWORDS: *cellulose nanocrystals, lignin, nanofibers, electrospinning, dynamic mechanical analysis, nanoindentation, thermomechanical properties, lignin films*
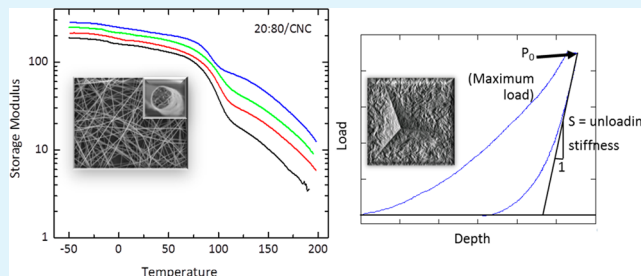
INTRODUCTION

We have reported on the synthesis of electrospun nanofibers from multicomponent systems including lignin, poly(vinyl alcohol) (PVA), and cellulose nanocrystals (CNCs). In particular, the properties of the precursor aqueous dispersions (viscosity, electroconductivity, and surface tension) were related to electrospinnability domains in composition maps and the resultant fiber properties.[1] Strong interactions, mainly intermolecular hydrogen bonding between hydroxyl groups of lignin and the PVA matrix as well as the dispersed CNCs, explained the improvement in the thermal properties of the multicomponent composite fibers compared to those of the respective single-phase systems.[1] Surface properties of the composite fibers containing lignin, PVA, and CNCs were also reported as far as the surface chemical composition, via X-ray photoelectron spectroscopy (XPS), space-resolved atomic force

microscopy (AFM)−thermal transitions, and water contact angle, which were used to examine the fiber structure, surface, and network properties.[2] Interestingly, at <50% lignin mass composition, the surface of lignin:PVA bicomponent electrospun fibers was covered with a thin layer of PVA; however, phase inversion was observed above this threshold value. The formation of phase-separated domains in the bicomponent electrospun fibers was influenced by the mass ratio of components and nonequilibrium solidification process because of the extremely fast evaporation under the high shear typical of electrospinning jet flow.

A number of reports indicate the improvement of the mechanical performance of electrospun fibers. In particular, incorporation of nanoparticles into precursor polymer systems has been used as one of the effective methods for fiber reinforcement.[3−5] Among these nanoparticles, several groups have proposed the incorporation of CNCs in composite fibers as a viable alternative for achieving remarkable reinforcing effects,[5−10] because of the CNC's high elastic modulus of 80−150 GPa in the axial direction and 10−50 GPa in the transverse direction.[11−14] In these cases, the beneficial effects of CNCs have been ascribed to a percolation effect, specifically, the result of interparticle interactions that tend to create a network at sufficiently high CNC loadings.[14−18]

In this investigation, we used isochronal dynamic mechanical analysis (DMA) to assess the storage modulus (E'), the loss modulus (E''), and the corresponding loss tangent (tan $\delta = E''/E'$) of lignin:PVA/CNC electrospun fiber mats between −50 and 200 °C. In addition to providing mechanical characterization, DMA measurements also provided information about the microphysical processes that are causally linked to the properties.[19] The aim of this work is to investigate the possibility of using lignin as a precursor for the manufacturing of carbon nanofibers that requires strength (dimensional stability) and a thermomechanical property, i.e., thermoplastic but a higher T_g for carbon fiber manufacturing, as well as a low cost.

To set the stage for further discussions, we show in Figure 1 the typical temperature-dependent viscoelastic behavior of
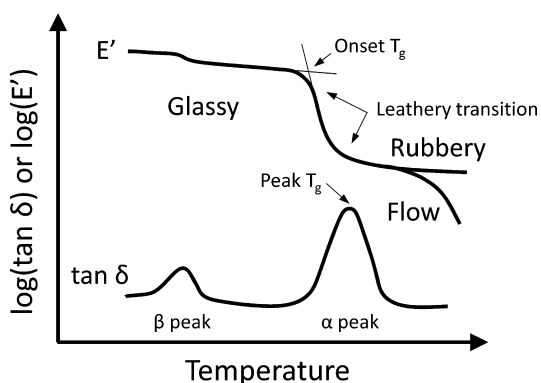

Figure 1. Characteristic temperature-dependent viscoelastic behavior of polymers as indicated in log(tan δ) and log(E') profiles as a function of temperature.

polymers over the range of temperatures studied. It includes a peak (β peak) in the low-temperature glassy region of the tan δ profile, corresponding to polymer side group motions. Only a slight decrease in E' is typically associated with this β relaxation. In the leathery transition, the α peak in the tan δ profile arises from the segmental motion within the polymer backbone, which causes a large decrease in the elastic modulus. The glass transition temperature (T_g) associated with this α peak is usually defined either at the onset of the decrease in the modulus or at the tan δ α peak. Both definitions have different meanings. The onset T_g represents the mechanical softening temperature and is most relevant when the polymer is used in load-bearing applications, whereas the tan δ peak corresponds to the temperature at which the polymers go through a mobility maximum. The rubbery region is assigned at temperatures above the T_g. If there is insufficient cross-linking or

entanglements, flow can occur at elevated temperatures. Here we used DMA viscoelastic characterization to study the effects of lignin, PVA, CNC, and relative humidity on the mechanical properties of the respective electrospun fiber mats. Thus, new insights into the molecular interactions causally linked to the properties were obtained.

The effects of the addition of CNCs on the elastic modulus (E_s^{NI}) and Meyer's hardness (H) of spin-coated lignin:PVA films were also investigated with nanoindentation on as-prepared surfaces and in cross section. Trends in E_s^{NI} were compared to the DMA's E' of fiber mats of the same composition to improve our understanding of the origins of their properties. The H results also provided insights into how the addition of CNCs affects the yield behavior of the composites. Nanoindentation has been used to study nano-fibers,[20−22] biological materials,[23,24] polymer composites,[25−27] nanocellulose,[28−30] and composite membranes consisting of poly(vinyl alcohol) and CNCs.[31] Despite the common use of nanoindentation to study polymer-based materials, proper experimental protocols and the meaning of E_s^{NI} and H are still debated in polymer science.[32−35] Standard nanoindentation protocols (i.e., the Oliver−Pharr method[36]) were developed for ceramic and metal materials that exhibit behavior different from that of polymers. Issues surrounding the assessment of contact area and viscoplasticity during unloading, the so-called "nose" effect, were recently addressed for polymers by Jakes and co-workers.[34] We follow their best practices and assess contact areas directly from residual indent images and applied a hold time at the maximal load prior to unloading to abate any potential forward viscoplastic deformation affecting the contact stiffness measurement of the unloading slope. We will also employ the structural compliance method[37] to account for and remove the effects of substrates, edges, and specimen-scale flexing in the nanoindentation measurements reported herewith.

■ EXPERIMENTAL SECTION

Materials. Lignin:PVA solutions and lignin:PVA/CNC dispersions were prepared according to the method described previously.[1] Lignin was obtained from Sigma-Aldrich (St. Louis, MO) with a reported molecular mass of 10 kDa (softwood alkali lignin, low sulfur, CAS registry number 8068-05-1). Poly(vinyl alcohol) (PVA) was acquired from the same supplier under trade name Mowiol 20-98 (CAS registry number 9002-89-5), with a reported molecular mass of 125 kDa and a degree of hydrolysis of 98% (2% acetyl group content). Lignin and PVA without further purification were used to prepare aqueous solutions for electrospinning.

Cellulose nanocrystals (CNCs) were prepared by acid hydrolysis of pure cotton fibers. Briefly, cotton was first acid hydrolyzed with 65 wt % sulfuric acid at 50 °C for 20 min. The resulting dispersion was poured into ∼500 g of ice cubes and washed with distilled water until the pH was neutral by successive centrifugation at 12000 rpm (10 °C for 20 min). Finally, dialysis for 1 week against deionized water with a 12000 molecular weight cutoff membrane (Spectrum Laboratories, Inc.) was performed to remove trace amounts of residual sulfuric acid from the suspension. The obtained CNCs (Figure S1a of the Supporting Information) were typically 100−150 nm in length and 10−20 nm in width, detected from the height image, in agreement with values reported in the literature.[11,38] The obtained CNC suspension was sonicated for 15 min to disperse any aggregated CNCs and kept refrigerated at 4 °C until it was used. The concentration of CNCs in the suspension was determined gravimetrically.

Multicomponent Electrospun Fibers. Aqueous PVA solutions (5 or 8 wt %) were prepared, and lignin was added to yield solutions with lignin:PVA dry mass ratios of 0:100, 20:80, 50:50, and 75:25.

Aqueous dispersions of 4.5 wt % CNCs were added to the lignin:PVA (20:80 and 75:25) solutions to yield dispersions with 5, 10, and 15 wt % CNCs based on total dry mass. The dispersions were kept under vigorous mechanical agitation at 60 °C for 15 min and then cooled to room temperature while being stirred for 120 min. Dispersions stored for less than one week were used to produce the electrospun fibers and spin-coated and solvent-casted films.

For electrospinning, the suspensions were loaded into a 10 mL plastic, disposable syringe with a 22 gauge needle. The needle was connected to the positive terminal of a voltage generator designed to produce a direct current voltage of up to 50 kV (Glassman High Voltage, Series EL). A thin aluminum foil covering a 15 cm diameter aluminum plate was used as a collector. The plate was connected to the negative electrode of the power supply (ground) and set at a working distance of 22 cm. An operating voltage of 19 kV was used. A constant flow rate of 8 μL/min was maintained during electrospinning using a computer-controlled syringe pump. Electrospinning was performed at room temperature and at 35−45% relative humidity. The collected electrospun mats were kept in a desiccator containing anhydrous $CaSO_4$.

Spin-Coated Film. Spin-coated films of lignin, PVA, and a lignin:PVA solution (75:25) with and without CNCs were deposited on top of silicon wafers. The silicon wafers (10 mm × 10 mm) were first cleaned thoroughly by immersion in a 10 wt % NaOH solution, rinsed with distilled water and ethanol, and finally subjected to UV−ozone treatment. The lignin, PVA, and lignin:PVA solutions were spin coated onto the silicon surfaces by first using 2000 rpm for 2.5 min followed by 700 rpm for 30 s. In the case of lignin:PVA/CNC dispersions, the second spinning stage was conducted at 1500 rpm for 15 s. The films were dried at room temperature for 8 h followed by vacuum drying at 40 °C for 12 h (see Figure 6 for atomic force microscopy images of spin-coated film surfaces).

Thermomechanical Analysis. The viscoelastic properties of the lignin:PVA and lignin:PVA/CNC fiber mats were evaluated from −50 to 200 °C in the linear elastic region using dynamic mechanical analysis (DMA) (model Q800, TA Instruments, New Castle, DE) under isochronal conditions at 1 Hz. The values of the storage modulus (E'), loss modulus (E''), and loss tangent (tan $\delta = E''/E'$) for a fixed frequency were obtained as a function of temperature. Extended electrospinning collection times were used to produce thick fiber mats suitable for DMA. The DMA measurements were performed in triplicate for each sample, and representative results are included here, noting that only negligible differences between samples were observed for a given condition.

Nanoindentation Experiments. Nanoindentation experiments were performed using a Hysitron (Minneapolis, MN) TI 900 TriboIndenter equipped with a Berkovich probe. The TriboIndenter was upgraded with a Performech controller. The elastic modulus (E_s^{NI}) and Meyer hardness (H) of three Lig:PVA/CNC spin-coated films (75:25 with 0, 5, and 15 wt % CNCs) were tested on the as-prepared surface and in cross section. The thickness of the spin-coated films varied within each film, and the thickest regions were chosen for testing. For as-prepared surface properties, 30 load-control 2 s−6 s−2 s load−hold−unload indents with maximal loads varying between 0.15 and 10 mN were used. The film thickness was constant over the area containing the indents. Substrate effects were accounted for using the structural compliance method as described in the Supporting Information.[37,39,40] In addition, E_s^{NI} and H were assessed in the cross section of the films. Small sections of films were separated from the silicon wafer substrate and mounted on a notched cylindrical steel slug with epoxy such that a portion of the film protruded above the slug. The steel slug was fit into the chuck of a Sorvall (Norwalk, CT) MT-2 ultramicrotome. The film cross-section surfaces were created by continuously removing thin sections (~300 nm) with a diamond knife until a sufficiently large area was prepared. From the cross sections, the films were found to be 30−50 μm thick. Because of the small film thickness, the structural compliance method[37,39,40] was employed to remove artifacts in nanoindentation measurements that can arise when free edges are near indents and specimen-scale flexing can occur. Indents placed in the film cross sections were force-control multiload

indents, consisting of ten 2 s−3 s−1.5 s−1 s partial load−hold at partial load−partial unload to 40% previous load−hold at partial unload cycles. The final hold at partial unload was 60 s and used to correct the load depth trace for thermal drift. Twenty multiload indents with maximal loads varying between 0.15 and 10 mN were placed in a row down the center of the cross section to maximize the distance from the free edges. During all experiments, the relative humidity was controlled by a water/glycerin bath inside the nanoindenter enclosure and ranged from 26 to 30%. The temperature was not actively controlled and ranged between 24 and 27 °C during the experiments. Standard protocols using a series of indents in a fused silica calibration standard were used to measure and remove machine compliance effects from experimental load depth traces. Further details about the assessment of E_s^{NI} and H and the structural compliance method are given in the Supporting Information.

Residual indents were imaged with a Quesant (Agoura Hills, CA) atomic force microscope incorporated into the TriboIndenter. The atomic force microscope was operated in contact mode and calibrated using an Advanced Surface Microscopy, Inc. (Indianapolis, IN), calibration standard as described previously.[37] Individual 10 μm field of view images were made of each indent. ImageJ (http://rsb.info.nih.gov/ij/) was used to manually measure the projected contact areas (A_0) using previously established methods.[34] Contact areas assessed from AFM images were used in the structural compliance method and the calculation of E_s^{NI} and H.

■ RESULTS AND DISCUSSION

Electrospun fibers based on lignin and poly(vinyl alcohol) (PVA) reinforced with cellulose nanocrystals (CNCs) were prepared from aqueous dispersions with given compositions. The concentrations of lignin and PVA are given as relative mass ratios in the respective fiber, and the percentage of CNC reported is based on total solids. For the sake of simplicity, we indicate such composition as "lignin:PVA/%CNC". Here emphasis is placed on multicomponent fibers electrospun from lignin:PVA solutions with two mass ratios, 20:80 and 75:25.

Thermomechanical Properties of Electrospun Lignin:PVA Fiber Mats. Figure 2 shows the temperature-dependent storage tensile modulus E' and tan δ for lignin:PVA bicomponent electrospun fiber mats, with the lignin concentration varying from 0 to 75 wt % of total solids. Table 1 includes summary data, including the fiber radius and glass transition temperature (T_g) (both peak T_g and onset T_g) and β peak. In the glassy region below 70 °C, the E' of PVA (0:100) electrospun fiber mats decreased slightly with temperature and a small β peak is observed in tan δ around −5 °C (Figure 2). The β peak is ~35 °C lower than that previously reported in the literature for PVA,[41] which is explained by the absorbed moisture.[41,42] In the glassy−rubbery transition, the E' of the fiber mat decreased ~1 order of magnitude; the onset T_g is estimated to be 78 °C, and the α peak T_g is estimated to be 95 °C.

At temperatures above the leathery transition, rubbery amorphous and crystalline domains coexisted for 0:100 lignin:PVA solutions and E' continued to decrease until it reached ~115 °C, at which point the measurement failed. In bulk PVA studies with other DMA analyses, flow was not observed at 115 °C;[41,42] thus, 115 °C is well below the melting temperature of PVA electrospun fibers of 229 °C, as examined by DSC experiments. Therefore, the measurement failure for the PVA electrospun fiber mat was likely an adhesion failure between fibers.

The E' in the glassy region below T_g generally decreased with an increasing weight percent of lignin (Figure 2). The modest
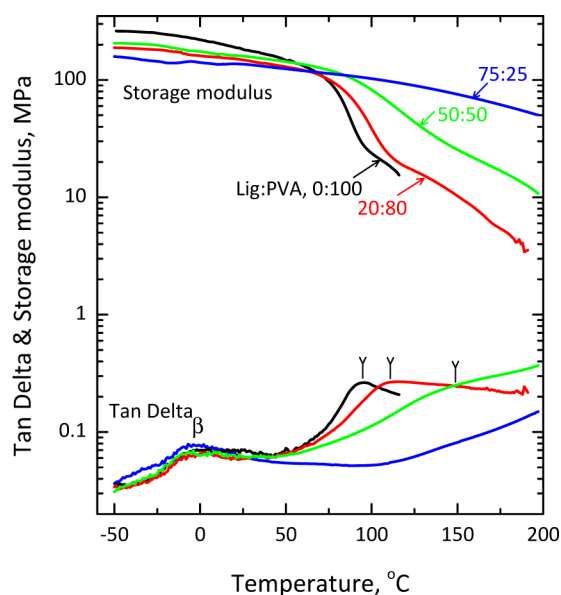
Figure 2. DMA storage tensile modulus E' and mechanical loss factor tan δ as a function of temperature for lignin:PVA electrospun fiber mats of various compositions, as indicated. The DMA experiments were conducted at a frequency of 1 Hz in the elastic region. The vertical arrows indicate the peak position of tan δ. The data were not normalized, and three repetitions were run for each condition, all showing similar profiles.

Table 1. Fiber Radii and Glass Transition Temperatures (T_g, peak T_g), Onset T_g Values, and β Peaks for Multicomponent (lignin:PVA/CNC) Electrospun Fibers As Determined in DMA Experiments

lignin:PVA/% CNC	β peak (°C)	onset T_g (°C)	T_g (°C)	peak T_g (°C) from tan δ
0:100/0	0	78	95	95
20:80/0	2	80	116	116
50:50/0	−5	82	166	166
75:25/0	−2	104	>200	>200
20:80/0	2	80	116	116
20:80/5	2	83	119	119
20:80/10	−1	84	159	159
20:80/15	2	81	104	104

reduction in E' in the glassy region can be attributed to an increased volume fraction of the amorphous lignin in the fibers, decreased PVA crystallinity, and changes in fiber mat density that caused changes in fiber radius (Table 1). The β peaks observed at 0, 2, −5, and 2 °C for 0:100, 20:80, 50:50, and 75:25 lignin:PVA fiber mats, respectively, result from the presence of small amounts of absorbed moisture in the samples;[42] the temperature and magnitude of the β peaks were nearly independent of the lignin:PVA ratio.

The most important features were noted in the leathery transition and rubbery region. For 20:80 lignin:PVA mats, the system did not fail until 190 °C; no failure was observed for the 50:50 and 75:25 lignin:PVA mats over the temperature range tested. The onset T_g values of 20:80 and 50:50 lignin:PVA mats were only a few degrees higher than that for pure PVA mats (Table 1), indicating that the PVA plays a controlling role in the glassy region. Interestingly, for the 75:25 lignin:PVA mat, the α relaxation was not observed in the studied temperature range despite the fact that the dry lignin T_g was estimated to be

in the range of 130−200 °C.[43,44] The lack of α relaxation suggests the molecular-scale interactions between lignin and PVA hinder the segmental motion and push the relaxation to higher temperatures. Also, the E' decreased by only ∼50% between −50 and 200 °C compared to the 2 order of magnitude decrease in E' for the 20:80 lignin:PVA fiber mat. The α peak T_g clearly shifted to higher temperatures, from 95 to 166 °C, for lignin weight percentages increasing from 0 to 50. In addition, the α peak broadened. This can be ascribed to the decrease in the PVA fraction in the matrix and the fact that the segmental motion of PVA in the amorphous regions is more restrained; therefore, a suppression of the α relaxation takes place because of the molecular interactions with lignin (via intermolecular hydrogen bonds).

Effect of CNC on the Viscoelastic Properties of Electrospun Fiber Mats. Figure 3 shows the E' and tan δ
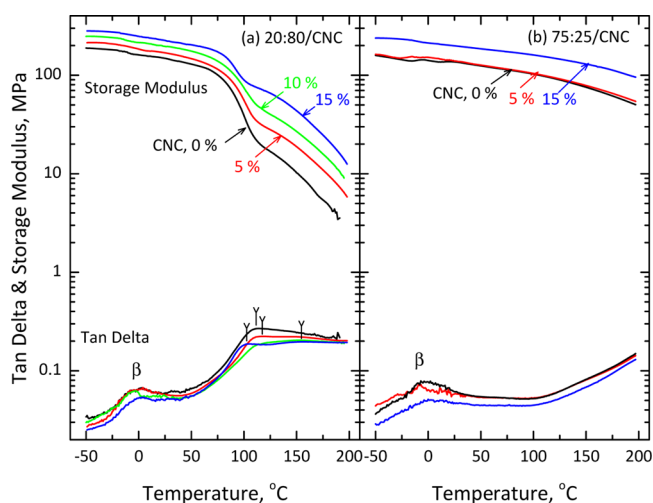

Figure 3. DMA storage tensile modulus E' and loss angle tangent, tan δ, as a function of temperature for lignin:PVA/CNC electrospun fiber mats: 20:80/%CNC (a) and 75:25/%CNC (b). The DMA experiments were conducted at a frequency of 1 Hz in the elastic region. The data were not normalized, and three repetitions were run for each condition, all showing similar profiles.

values as a function of temperature for 20:80/%CNC and 75:25/%CNC systems with 5, 10 (for only the 20:80 system), and 15 wt % CNCs. In the tan δ profile, a small β peak, similar to what was observed in bicomponent (lignin:PVA) systems (Figure 2 and Table 1), was recorded for 20:80/%CNC mats at 2, −1, and 2 °C with increased CNC content. In the glassy region, below 80 °C, the E' of the 20:80/%CNC systems increased modestly with CNC loading. The onset T_g of the 20:80/%CNC mats remained constant, 80 °C, for the different CNC loadings. However, in the temperature range from 80 to 95 °C, the tan δ peak T_g values were affected and the magnitude of the α peak was substantially suppressed, and the E' values increased with an increased weight percent of CNC (Figure 3a). The observed phenomenon indicates a decrease in the amount of mobile matrix participating in the relaxation process and the accommodation of the reinforcing, rigid CNC particles.[45] The E' in the rubbery region was also affected by the degree of crystallinity and morphology of the matrix. In the 20:80/%CNC system, the degree of crystallinity of PVA, which was reported from DSC measurements in our previous study,[1] decreased with an increased concentration of the dispersed CNCs. Therefore, it is concluded that the observed enhance-

ment of the storage modulus in multicomponent fiber mats can be directly related to the reinforcing effect of the dispersed CNCs, i.e., by the interconnected network formed and held by hydrogen bonds.[14,16−18]

Figure 3a shows tan δ profiles as a function of temperature for the 20:80/%CNC system. The position of the temperature peak corresponding to the leathery transition shifted to higher values, from 116 to 159 °C, and the magnitude of the peak decreased with CNC loading up to 10% (Table 1). This effect is related to the presence of strong interactions, i.e., hydrogen bonding between hydroxyl groups of the polymeric matrix and the CNCs, which causes restricted molecular mobility. As discussed previously, intermolecular interaction via hydrogen bonds between the matrix and the CNCs in multicomponent systems is an important factor contributing to the improved mechanical and thermal properties.[1] The reinforcing effect of CNCs and the composition dependence are consistent with the effective stress transfer occurring between the matrices and CNCs. When 15 wt % CNCs was present in the composite fiber, the maximal peak of tan δ profiles slightly decreased to 104 °C. This observation can be related to (i) filler−filler slippage or friction, (ii) particle−polymer motion at the filler interface, and (iii) a change in the properties of the polymer by adsorption onto the reinforcing particles.[46]

For 75:25/%CNC systems, no significant influence of addition of 5 wt % CNCs was observed on the storage modulus and peak of tan δ (Figure 3b). At 15 wt % CNCs, however, a large increase in the storage modulus was observed over the whole temperature range. This fact indicates that the mechanical behavior of the composite matrix is influenced by the reinforcing phase at a given weight percentage of CNC threshold value because of the percolation threshold as described below. It is worth noting that compared to the unfilled fibers, the fibers loaded with 15 wt % CNCs had a larger diameter (148 ± 4 nm for unfilled and 194 ± 7 nm for 15 wt % CNCs), which in turn indicates that the density of the fiber mat may have decreased. If only the density and the number of fiber contacts were taken into account, the strength of the mats would have been expected to decrease with CNC load. Therefore, the fact that the storage modulus of the 25:75/15% fiber mats was enhanced can be taken as unequivocal evidence of the reinforcing effect of CNCs. Without normalizing the DMA elastic modulus for mat density, one can argue that interpretation of the changes in the magnitude of the elastic modulus is difficult. For example, it can be assumed that changes in the modulus could be caused by changes in fiber mechanical properties, mat density, or mat structure (i.e., number of entanglements, fiber adhesion, etc.). We already have shown that the crystallinity of PVA in the composite fiber was reduced upon addition of CNCs.[1] However, as noted above, a critical fact that confirms the reinforcing effect is that CNC addition actually increases fiber radius, which would otherwise reduce the mechanical strength of the mat. The 75:25/15% lignin:PVA/CNC fiber mat maintained its mechanical properties fairly well over a wide range of temperatures.

The origin of the CNC reinforcing effect has been highlighted for many systems, especially films, and related to the mechanical percolation effects occurring above a threshold, expected to be around few percent units for such rodlike particles, depending on their aspect ratio.[16,17,47−50] As such, it is of interest to compare the performance of the lignin:PVA/CNC fibers to the data predicted from a model based on the percolation concept. As such, we calculated the modulus of the

multicomponent fibers by using a percolation model that Favier et al.[16−18] applied to poly(S-co-BuA) reinforced with (tunicin) CNCs. It was found that above a percolation threshold concentration, the cellulosic nanoparticles formed a strongly interacting three-dimensional continuous network throughout the nanocomposite film.[16−18] In this case, the model failed to describe the experimental modulus in the rubbery state (Figure 4). Noticeably, the experimental values of the modulus of the
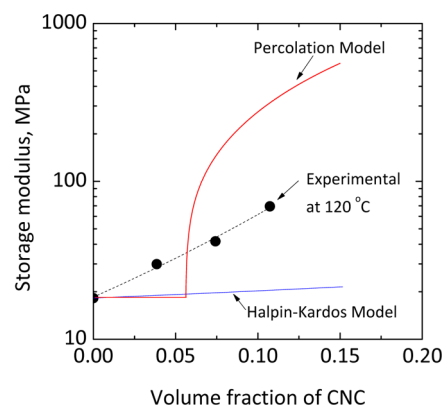

Figure 4. Comparison of reinforced composite models and the DMA storage moduli of lignin:PVA/CNC at various CNC volume fractions. The plots represent the experimental results above the glass transition temperature at 120 °C, and the solid lines are the percolation model used in refs 16−18 and the Halpin−Kardos model.[15]

electrospun fibers reinforced with CNCs were much higher than the values calculated by the Halpin−Kardos model[15] after considering negligible interactions between fillers. This observation provides further support to the hypothesis that the enhancement of the mechanical strength of the electrospun fiber mats is the result of the formation of a network between CNCs at the given loading.

Effect of Humidity. Experiments were performed with electrospun fiber mats that were first conditioned in a humid atmosphere (97% relative humidity) and then dried under vacuum at 40 °C. It was observed that the storage modulus of the CNC-free systems increased for all temperatures (Figure 5a).

After samples had been conditioned at 97% relative humidity (RH), water plasticized some of the amorphous polymers, increasing their molecular mobility with deformation hydrogen
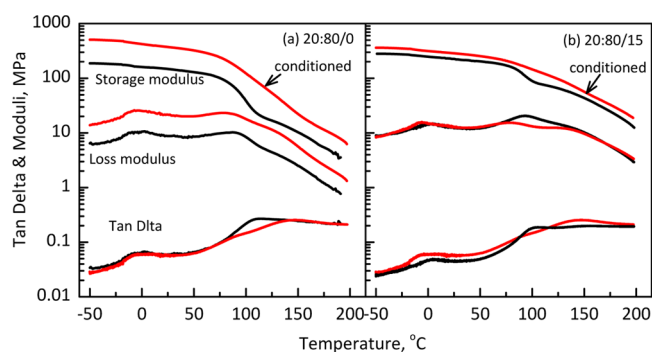

Figure 5. Storage and loss moduli and tan δ for 20:80/0% CNC (a) and 20:80/15% CNC (b) before (black) and after (red) conditioning in ambient air at 97% relative humidity. All the samples were vacuum-dried at 40 °C for 4 h.

bonding between CNCs and/or CNCs and the matrix. The rate of removal of water during vacuum drying is much slower than during electrospinning, and the plasticized amorphous polymers have an opportunity to reach a lower-energy state configuration. The result is a material with a higher modulus. The effect of relative humidity conditioning on the CNC-loaded mat is weaker because of the molecular interactions with the CNCs.[12,51,52] The α peak T_g is also observed to increase after RH conditioning, further suggesting the polymers achieve a more energetically favorable configuration after RH conditioning (Figure 5b). In some ways, RH conditioning is like temperature annealing in polymers.

Nanoindentation. Nanoindentation was used to assess the elastic modulus (E_s^{NI}) and Meyer hardness (H) of spin-coated 75:25 (lignin:PVA) films with 0, 5, and 15 wt % CNCs. Both the as-prepared film surfaces and surfaces prepared in cross section were tested. For nanoindentation analyses, contact areas (A_0) were assessed from high-resolution AFM images of residual indents (similar to Figure 6a−e) following established
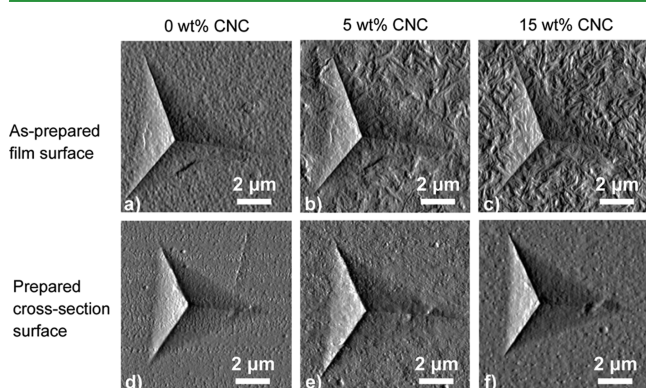

Figure 6. Atomic force microscopy images of residual 9.5 mN indent impressions in 75:25 lignin:PVA spin-coated films on the as-prepared film surface (a−c) and the surface prepared in cross section (d−f) with 0 wt % CNCs (a and d), 5 wt % CNCs (b and e), and 15 wt % CNCs (c and f).

protocols.[34] Meyer hardness H, defined as the maximal load immediately prior to unloading divided by A_0, is plotted as a function of indent size ($A_0^{1/2}$) in Figure 7 for all surfaces tested. An indentation size effect was observed with H decreasing with an increasing indent size. The H indentation size effect is not an artifact caused by the substrate−film interface beneath the as-prepared surface nanoindents or free edges near the cross-section nanoindents because the plastic zone beneath the Berkovich probe was much too small to overlap the substrate−film interface or free edges. An upper estimate of the radius of the plastic zone beneath a Berkovich probe for our largest indents was 6 μm,[53] which was much smaller than the film thicknesses (>30 μm). Furthermore, a method for verifying the presence of an indentation size effect is to determine the structural compliance (C_s) using both the Doerner−Nix (DN) plot[54] and the Stone−Yoder−Sproul (SYS) correlation.[55] The C_s, which is consistently lower from the SYS method than from the DN method (Table 2), strongly supports the observed H indentation size effect in Figure 7. Using the same experimental methods, no H indentation size effect was observed in the glassy polymers poly(methyl methacrylate), polystyrene, and polycarbonate over a similar range of indent sizes.[35] The magnitude of the indentation size effect, as indicated by the slope of a straight line fit to the H data in Figure 7, $dH/dA_0^{1/2}$,
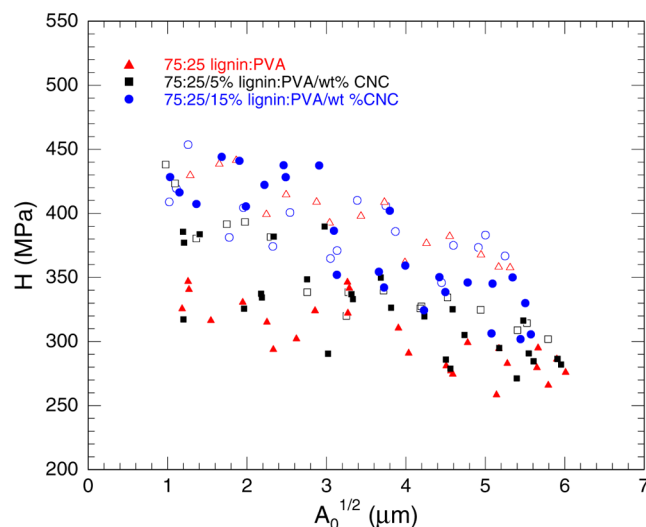

Figure 7. Meyer hardness (H) as a function of indent size (square root of contact area, $A_0^{1/2}$) for 75:25 lignin:PVA spin-coated films on the as-prepared film surface (filled symbols) and surface prepared in cross section (empty symbols) with 0 wt % CNCs (red triangles), 5 wt % CNCs (black squares), and 15 wt % CNCs (blue circles).

is also included in Table 2. For comparison, the average H assessed at $A_0^{1/2}$ values from 3 to 5 μm was used (Table 2). To remove substrate effects in the as-prepared surface nanoindents, and the effects of edges and specimen-scale flexing in the cross-section nanoindents, the structural compliance method[39,40,56] was used in the assessment of E_s^{NI}. E_s^{NI} was calculated directly from the slope of a DN plot and from individual load depth traces corrected using the DN C_s. Both methods for calculating E_s^{NI} gave similar results (Table 2). The experimental DN and SYS plots and additional details of the nanoindentation analyses are given in the Supporting Information.

On the as-prepared surface, increasing amounts of CNCs are observed in the AFM images with increasing loading (Figure 6a−c). The as-prepared surface E_s^{NI} increases from 5.9 GPa to 6.5 and 7.3 GPa upon addition of 5 and 15 wt % CNCs, respectively. The increase is approximately the amount expected for a simple mixing rule. If one assumes the matrix modulus is 5.9 GPa and all the CNCs are uniformly distributed, lying parallel to the film surface with a 15 GPa transverse modulus,[57] then the composite modulus upon addition of 5 and 15% CNCs would be ~6.4 and ~7.3 GPa, respectively. For nanoindents in the cross section (Figure 6d−f), no effect of addition of 5 wt % CNCs on E_s^{NI} was observed with 6.8 and 6.6 GPa for 0 and 5 wt %, respectively. Upon addition of 15 wt % CNCs, E_s^{NI} increased to 8.4 GPa. The trend in cross-section E_s^{NI} resembles the trend in E' in Figure 3b for 75:25 lignin:PVA composites with CNC addition, suggesting the spin-coated cross-section E_s^{NI} is more closely related to electrospun fiber mat E' than as-prepared film surface E_s^{NI}. On the as-prepared surface, H increased from 310 MPa with 0 wt % CNCs to 320 and 360 MPa with 5 and 15 wt % CNCs, respectively, showing that with increasing amounts of CNCs the resistance of the surfaces to plastic deformation is improved. In contrast, the cross section has a H of 390 MPa with 0 wt % CNCs, which then decreases to 330 MPa upon addition of 5 wt % CNCs and increases back to 380 MPa upon addition of 15 wt % CNCs. The decrease in H upon addition of 5 wt % CNCs in the cross section suggests that the CNCs might be creating weak interfaces between the composite domains. The weak interfaces

Table 2. Data from a Series of Indents Performed on the As-Prepared Surface and Surface Prepared in Cross Section of 75:25 Lignin:PVA Spin-Coated Films Reinforced with 5 or 15 wt % CNCs

		SYS	DN			from individual indents			
		C_s (μm/N)	C_s (μm/N)	E_s from the DN slope (GPa)	E_s with DN C_s (GPa)	H ($A_0^{1/2}$ from 3 to 5 μm) (MPa)	$dH/dA_0^{1/2}$ (MPa/μm)	n
as-prepared surface	75:25	-4.2 ± 0.4^a	-1.3 ± 0.7^a	5.9 ± 0.1^a	5.9 ± 0.1^b	310 ± 10^b	-13 ± 2^a	27
	75:25/5	-4.6 ± 0.4^a	-0.9 ± 0.5^a	6.5 ± 0.1^a	6.5 ± 0.1^b	320 ± 10^b	-18 ± 3^a	27
	75:25/15	-3.7 ± 0.5^a	-0.4 ± 0.8^a	7.3 ± 0.1^a	7.3 ± 0.1^b	360 ± 10^b	-28 ± 3^a	26
cross section	75:25	12.3 ± 0.5^a	15.7 ± 0.6^a	6.8 ± 0.1^a	6.8 ± 0.1^b	390 ± 10^b	-19 ± 2^a	15
	75:25/5	11.9 ± 0.3^a	16.7 ± 0.6^a	6.6 ± 0.2^a	6.6 ± 0.1^b	330 ± 10^b	-23 ± 3^a	17
	75:25/15	10.6 ± 0.4^a	12.2 ± 1.1^a	8.3 ± 0.2^a	8.4 ± 0.1^b	380 ± 10^b	-12 ± 4^a	17

[a]Uncertanties based on least-squares analysis for corresponding linear fits. [b]Uncertainties based on the standard error.

might also explain why no increase in E_s^{NI} or E' was achieved with the 75:25/5 lignin:PVA/CNC composites.

The H and corresponding indentation size effect may also provide insights into the microphysical processes controlling the yield beneath the nanoindentation probe. The composite has a very complex microstructure. In our previous work, we used scanning electron microscopy (SEM) to image cross sections prepared by freeze fracturing of 25:75 lignin:PVA solvent-casted films with 0, 5, and 15 wt % CNCs.[2] The SEM images showed distinct phase-separated domains as large as 0.5 μm. The domain sizes varied with the film thickness, and the domain size decreased upon addition of CNC. Furthermore, using AFM-based local thermal analysis, both lignin- and PVA-rich domains were identified.[2] Although evaporation rates are much higher in spin coating than in solvent casting, similar trends in microstructure should be expected in the spin-coated films studied here. The complex microstructure leads to many potential processes that could be contributing to yield strength. If an indent is small and the plastic zone is contained within a small number of phase-separated domains, yielding is likely controlled through the initiation and propagation of shear transformation zones within a domain if it is amorphous or dislocations if it is crystalline.[58] As the size of the indent increases and the plastic zone encompasses many phase-separated domains, the properties of the interphase regions between the domains may dominate the yield. If the interphase regions are weak, it might lead to a decreasing H with an increased indent size as the interphase regions play a larger role. The change in the process controlling the yield is one possible explanation for the H indentation size effect. The addition of the strong CNCs further complicates the potential yield processes, and it would be expected that strong CNC−matrix interactions would lead to an increase in composite yield strength and weak interactions may lead to a decrease in yield strength. On the as-prepared surface, H increases upon addition of CNCs, suggesting good CNC−matrix interactions at the surface. Also, the magnitude of the indentation size effect increased upon addition of CNCs, suggesting either a higher concentration of CNCs at the surface or the fact that the processes controlling the yield changed with both depth and CNC addition. In contrast, H in the cross sections decreased after addition of 5 wt % CNCs and increased again after addition of 15 wt % CNCs. However, upon closer inspection of the data in Figure 6, we observed that for the smallest indents H is similar after addition of both 5 and 15 wt % CNCs. The 5 wt % CNC load has a much larger indentation size effect than the 15 wt % CNC composite. If the addition of 5 wt % CNCs causes weak interfaces, as the E_s^{NI} or E' results suggest, this may

explain why the cross-section H decreases for the larger indents in the 5 wt % CNC cross section as the interphase regions play a larger role in controlling the yield strength.

Differences between as-prepared surface and cross-section E_s^{NI} and H were observed even in composites without CNCs. Both E_s^{NI} and H were substantially higher in cross section than on the as-prepared surface for the film with 0 wt % CNCs. After addition of 5 wt % CNCs, the as-prepared surface and cross section have similar E_s^{NI} and H values, with the values for the as-prepared surface increasing and the values for the cross section decreasing. E_s^{NI} and H increased similarly on both surfaces after addition of 15 wt % CNCs. The different behaviors of the two surfaces suggest anisotropy that could be caused by a preferential orientation of CNCs, composition gradients, or inhomogeneous microstructures in the film. The gradients in microstructure and composition may be caused by differences in evaporation rates through the spin-coated film thicknesses. It is important to note that with respect to addition of CNCs only the trend in cross-section E_s^{NI} resembled the trend in DMA E'. Therefore, testing only the as-prepared surface would have been insufficient to accurately predict the trend in the fiber mat properties.

Because the trend in the cross-section E_s^{NI} is similar to that of DMA E' with the 75:25 system, it can be inferred that changes in DMA E' of fiber mats predominantly arise from changes in fiber properties. For the 20:80 systems, such an interpretation may be challenging because the effect of addition of CNCs may differently affect the two systems. This is because there is likely a competing effect upon addition of CNCs: they lead to a lowering of the PVA crystallinity, which would lower the modulus but also increases the composite modulus because of the stiff nature of the reinforcing nanoparticles. Details about the nature of this phenomenon are outside the scope of this discussion, however.

■ CONCLUSIONS

Defect-free electrospun fibers were produced from aqueous dispersions of lignin, poly(vinyl alcohol) (PVA) (20:80 and 75:25 lignin:PVA), and cellulose nanocrystals (CNCs, 0, 5, 10, and 15 wt %) as the reinforcing solid phase. The mechanical properties of lignin:PVA/CNC electrospun fiber mats and spin-casted films were investigated by DMA and nanoindentation, respectively. The DMA results revealed that the thermomechanical performance of lignin:PVA electrospun mats was improved upon addition of lignin, because of the strong molecular interaction with PVA. The addition of CNCs further improved such properties. It was observed that CNCs also lead to the stabilization of the matrix against water absorption.

Nanoindentation of as-prepared spin-coated films showed that both E_s^{NI} and H increased upon addition of CNCs. However, in cross section, E_s^{NI} and H initially decreased with 5 wt % CNCs and then increased after addition of 15 wt % CNCs, suggesting weak interphase regions with addition of only 5 wt % CNCs. DMA E' and cross-section E_s^{NI} had the same trend with respect to addition of CNCs, indicating it is necessary to test spin-coated film cross sections to correctly predict how changes in composition will translate to changes in fiber mat properties. The indentation size effect in H suggests there are multiple competing processes controlling the yield beneath the probe, and the dominant process depends on the size of the nanoindent. These results support evidence of the molecular interaction as well as efficient stress transfer between the lignin:PVA matrix and dispersed CNCs.

ASSOCIATED CONTENT

Ⓢ Supporting Information

Morphological analyses and nanoindentation tests as described in the text. This material is available free of charge via the Internet at http://pubs.acs.org.

AUTHOR INFORMATION

Corresponding Authors
*E-mail: ago@fe.bunri-u.ac.jp.
*E-mail: jjakes@fs.fed.us.

Notes
The authors declare no competing financial interest.

ACKNOWLEDGMENTS

REFERENCES

(1) Ago, M.; Okajima, K.; Jakes, J. E.; Park, S.; Rojas, O. J. *Biomacromolecules* **2012**, *13*, 918−926.

(2) Ago, M.; Jakes, J. E.; Johansson, L.-S.; Park, S.; Rojas, O. J. *ACS Appl. Mater. Interfaces* **2012**, *4*, 6849−6856.

(3) Lu, X.; Wang, C.; Wei, Y. *Small* **2009**, *5*, 2349−2370.

(4) Ji, J.; Sui, G.; Yu, Y.; Liu, Y.; Lin, Y.; Du, Z.; Ryu, S.; Yang, X. *J. Phys. Chem. C* **2009**, *113*, 4779−4785.

(5) Park, W.-I.; Kang, M.; Kim, H.-S.; Jin, H.-J. *Macromol. Symp.* **2007**, *249−250*, 289−294.

(6) Peresin, M. S.; Habibi, Y.; Zoppe, J. O.; Pawlak, J. J.; Rojas, O. J. *Biomacromolecules* **2010**, *11*, 674−681.

(7) Zoppe, J. O.; Peresin, M. S.; Habibi, Y.; Venditti, R. A.; Rojas, O. J. *ACS Appl. Mater. Interfaces* **2009**, *1*, 1996−2004.

(8) Ping, L.; You-Lo, H. *Nanotechnology* **2009**, *20*, 415604.

(9) Zhou, C.; Chu, R.; Wu, R.; Wu, Q. *Biomacromolecules* **2011**, *12*, 2617−2625.

(10) Rojas, O. J.; Montero, G. A.; Habibi, Y. *J. Appl. Polym. Sci.* **2009**, *113*, 927−935.

(11) Elazzouzi-Hafraoui, S.; Nishiyama, Y.; Putaux, J.-L.; Heux, L.; Dubreuil, F.; Rochas, C. *Biomacromolecules* **2008**, *9*, 57−65.

(12) Garcia de Rodriguez, N. L.; Thielemans, W.; Dufresne, A. *Cellulose* **2006**, *13*, 261−270.

(13) Habibi, Y.; Hoeger, I.; Kelley, S. S.; Rojas, O. J. *Langmuir* **2010**, *26*, 990−1001.

(14) Habibi, Y.; Lucia, L. A.; Rojas, O. J. *Chem. Rev.* **2010**, *110*, 3479−3500.

(15) Halpin, J. C.; Kardos, J. L. *J. Appl. Phys.* **1972**, *43*, 2235−2241.

(16) Favier, V.; Canova, G. R.; Cavaillé, J. Y.; Chanzy, H.; Dufresne, A.; Gauthier, C. *Polym. Adv. Technol.* **1995**, *6*, 351−355.

(17) Favier, V.; Chanzy, H.; Cavaille, J. Y. *Macromolecules* **1995**, *28*, 6365−6367.

(18) Favier, V.; Cavaille, J. Y.; Canova, G. R.; Shrivastava, S. C. *Polym. Eng. Sci.* **1997**, *37*, 1732−1739.

(19) Lakes, R. S. *Viscoelastic materials*; Cambridge University Press: New York, 2009.

(20) Li, X.; Gao, H.; Murphy, C. J.; Caswell, K. K. *Nano Lett.* **2003**, *3*, 1495−1498.

(21) Tan, E. P. S.; Lim, C. T. *Appl. Phys. Lett.* **2005**, *87*, 123106-3.

(22) Ko, F.; Gogotsi, Y.; Ali, A.; Naguib, N.; Ye, H.; Yang, G. L.; Li, C.; Willis, P. *Adv. Mater.* **2003**, *15*, 1161−1165.

(23) Ebenstein, D. M.; Pruitt, L. A. *Nano Today* **2006**, *1*, 26−33.

(24) Jakes, J. E.; Bechle, N. J.; Hamel, S.; Gronvold, A. G.; Hermanson, J. C.; Stone, D. S. Investigating Deformation in HDPE-Wood Flour Composites Using Uniaxial Tension and Nano-indentation Experiments. In *Tenth International Conference on Wood & Biofiber Plastic Composites and Cellulose Nanocomposites Sysmposium*, Madison, WI, May 11−12, 2009; Research and Markets: Dublin, 2010; pp 121−125.

(25) Van Meerbeek, B.; Willems, G.; Celis, J. P.; Roos, J. R.; Braem, M.; Lambrechts, P.; Vanherle, G. *J. Dent. Res.* **1993**, *72*, 1434−1442.

(26) Lee, S.-H.; Wang, S.; Pharr, G. M.; Xu, H. *Composites, Part A* **2007**, *38*, 1517−1524.

(27) VanLandingham, M. R.; Villarrubia, J. S.; Guthrie, W. F.; Meyers, G. F. *Macromol. Symp.* **2001**, *167*, 15−44.

(28) Lahiji, R. R.; Xu, X.; Reifenberger, R.; Raman, A.; Rudie, A.; Moon, R. J. *Langmuir* **2010**, *26*, 4480−4488.

(29) Jakes, J. E.; Baez, C. L.; Rowlands, R. E.; Considine, J. M.; Stone, D. S. Applications of nanoindentation-based mechanical spectroscopy in forest products research. 2011 TAPPI International Conference on Nanotechnology for Renewable Materials, Arlington, VA, June 6−8, 2011.

(30) Pakzad, A.; Simonsen, J.; Heiden, P. A.; Yassar, R. S. *J. Mater. Res.* **2012**, *27*, 528−536.

(31) Pakzad, A.; Simonsen, J.; Yassar, R. S. *Nanotechnology* **2012**, *23*, 085706.

(32) Oyen, M. L.; Cook, R. F. *J. Mater. Res.* **2003**, *18*, 139−150.

(33) VanLandingham, M. R.; Chang, N. K.; Drzal, P. L.; White, C. C.; Chang, S. H. *J. Polym. Sci., Part B: Polym. Phys.* **2005**, *43*, 1794−1811.

(34) Jakes, J. E.; Lakes, R. S.; Stone, D. S. *J. Mater. Res.* **2012**, *27*, 463−474.

(35) Jakes, J. E.; Lakes, R. S.; Stone, D. S. *J. Mater. Res.* **2012**, *27*, 475−484.

(36) Oliver, W. C.; Pharr, G. M. *J. Mater. Res.* **1992**, *7*, 1564−1583.

(37) Jakes, J. E.; Frihart, C. R.; Beecher, J. F.; Moon, R. J.; Stone, D. S. *J. Mater. Res.* **2008**, *23*, 1113−1127.

(38) Ebeling, T.; Paillet, M.; Borsali, R.; Diat, O.; Dufresne, A.; Cavaillé, J. Y.; Chanzy, H. *Langmuir* **1999**, *15*, 6123−6126.

(39) Jakes, J. E.; Frihart, C. R.; Beecher, J. F.; Moon, R. J.; Resto, P. J.; Melgarejo, Z. H.; Suárez, O. M.; Baumgart, H.; Elmustafa, A. A.; Stone, D. S. *J. Mater. Res.* **2009**, *24*, 1016−1031.

(40) Jakes, J. E.; Stone, D. S. *Philos. Mag.* **2010**, *91*, 1387−1399.

(41) McCrum, N. G.; Read, B. E.; Williams, G. In *Anelastic and dielectric effects in polymeric solids*; Dover Publications: New York, 1991; pp 327−343.

(42) Cendoya, I.; López, D.; Alegría, A.; Mijangos, C. *J. Polym. Sci., Part B: Polym. Phys.* **2001**, *39*, 1968−1975.

(43) Back, E. L.; Salmén, L. *Glass transitions of wood components hold implications for molding and pulping processes*; Svenska träforskningsinstitutet: Stockholm, 1982.

(44) Kelley, S.; Rials, T.; Glasser, W. *J. Mater. Sci.* **1987**, *22*, 617−624.

(45) Hubbe, M. A.; Rojas, O. J.; Lucia, L. A.; Sain, M. *BioResources* **2008**, *3*, 929−980.

(46) Kim, J.; Montero, G.; Habibi, Y.; Hinestroza, J. P.; Genzer, J.; Argyropoulos, D. S.; Rojas, O. J. *Polym. Eng. Sci.* **2009**, *49*, 2054−2061.

(47) Azizi Samir, M. A. S.; Alloin, F.; Gorecki, W.; Sanchez, J.-Y.; Dufresne, A. *J. Phys. Chem. B* **2004**, *108*, 10845−10852.

(48) Dubief, D.; Samain, E.; Dufresne, A. *Macromolecules* **1999**, *32*, 5765−5771.

(49) Dufresne, A.; Kellerhals, M. B.; Witholt, B. *Macromolecules* **1999**, *32*, 7396−7401.

(50) Dufresne, A. *Compos. Interfaces* **2000**, *7*, 53−67.

(51) Peresin, M. S.; Habibi, Y.; Vesterinen, A.-H.; Rojas, O. J.; Pawlak, J. J.; Seppälä, J. V. *Biomacromolecules* **2010**, *11*, 2471−2477.

(52) Mathew, A. P.; Dufresne, A. *Biomacromolecules* **2002**, *3*, 609−617.

(53) Chen, J.; Bull, S. J. *Surf. Coat. Technol.* **2006**, *201*, 4289−4293.

(54) Doerner, M. F.; Nix, W. D. *J. Mater. Res.* **1986**, *1*, 601−609.

(55) Stone, D. S.; Yoder, K. B.; Sproul, W. D. *J. Vac. Sci. Technol., A* **1991**, *9*, 2543−2547.

(56) Jakes, J. E.; Frihart, C. R.; Beecher, J. F.; Moon, R. J.; Stone, D. S. *J. Mater. Res.* **2008**, *23*, 1113−1127.

(57) Moon, R. J.; Martini, A.; Nairn, J.; Simonsen, J.; Youngblood, J. *Chem. Soc. Rev.* **2011**, *40*, 3941−3994.

(58) Oleinik, E. F.; Rudnev, S. N.; Salamatina, O. B. *Polym. Sci., Ser. A* **2007**, *49*, 1302−1327.